Internuclear distance measurements up to 0.44 nm for retinals in the solid state with 1-D rotational resonance C-13 MAS NMR spectroscopy

Verdegem, P.J.E.; Helmle, M.; Lugtenburg, J.; Groot, H.J.M. de

Note: To cite this publication please use the final published version (if applicable).

J. Am. Chem. Soc. **1997,** *119,* 169−174

169

Internuclear Distance Measurements up to 0.44 nm for Retinals in the Solid State with 1-D Rotational Resonance ^{13}C MAS NMR Spectroscopy

P. J. E. Verdegem, M. Helmle, J. Lugtenburg, and H. J. M. de Groot*

Contribution from Gorlaeus Laboratories, Leiden Institute of Chemistry, Leiden University, P.O. Box 9502, 2300 RA Leiden, The Netherlands

Received May 3, 1996[⊗]

Abstract: The results presented in this paper show that accurate through-space internuclear distance measurements can be performed on doubly labeled retinals using the one-dimensional approach to the solid state magic angle spinning (MAS) rotational resonance NMR technique. The apparent splitting $\Delta\omega_1$ of the resonances at $n = 1$ rotational resonance for the labeled vinylic positions of (*all-E*)-[10,20-^{13}C$_2$]retinal, (*all-E*)-[11,20-^{13}C$_2$]retinal, and (*all-E*)-[12,20-^{13}C$_2$]retinal can be simulated with a coherent set of parameters. From a series of simulations with different dipolar coupling constant b_{IS}, it appears that $b_{IS}/2\pi\sqrt{8} = 1.15(\Delta\omega_1/2\pi) + 7$ (Hz) to a good approximation. Using this relationship as a calibration, it is demonstrated with a set of model compounds that straightforward Lorentzian fitting to measure $\Delta\omega_1$ can be used to determine internuclear distances up to 0.44 nm in doubly labeled retinals in the solid state.

Rotational resonance is a high-resolution solid state magic angle spinning (MAS) NMR technique in which the interference of the MAS with the homonuclear dipole interactions within a pair of equal spins I and S gives rise to dipolar recoupling.[1,2] This phenomenon can be exploited to measure the internuclear distance. The rotation frequency of the sample ω_r is adjusted to match a rotational resonance condition $n\omega_r = \Delta\omega_{IS}$ with $\Delta\omega_{IS} = \omega_I - \omega_S$, the difference between the isotropic shifts. With n a small integer and a homonuclear dipolar coupling

$$B_{IS} = \left| -\left(\frac{\mu_0}{4\pi}\right)\frac{\gamma^2\hbar}{r_{IS}^3} \right| \quad (1)$$

sufficiently strong compared to the average linewidths Γ, the line shapes change at or close to a rotational resonance condition and additional fine structure or broadening can be observed. In eq 1 μ_0 is the magnetic permeability in vacuum, γ is the gyromagnetic ratio of the nuclei, and r_{IS} represents the internuclear distance. To a first-order approximation, neglecting the influence of anisotropy and relaxation effects, an apparent splitting $\Delta\omega_n$ of each resonance is expected.[1] At or close to $n = 1$ rotational resonance the spectrum of a doubly labeled sample can be described by

$$S(\omega) = \frac{1}{16\pi b_{IS}}\sum_{M=1}^{8} Y^{(1)}\left(\frac{\Omega_M(\omega)}{b_{IS}/(2\sqrt{8})}\right) \quad (2)$$

with $\Omega_M(\omega)$ the set of frequency offset functions for the eight spectral components and

$$Y^{(1)}(x) = \left[\frac{1}{(1-x^2)^{1/2}} + 1\right]^{1/2} + \left[\frac{1}{(1-x^2)^{1/2}} - 1\right]^{1/2} \quad (3)$$

the line shape function,[1] which is only evaluated for $0 < |x| <$

1. The extrema of the spectrum can be found at the positions where $x = 1$ or $x = -1$; in these cases the line shape function goes to infinity. In the absence of *J*-coupling these singularities can be found at $\omega = \omega_I \pm b_{IS}/2\sqrt{8}$ and $\omega = \omega_S \pm b_{IS}/2\sqrt{8}$, predicting a "splitting" in the line shape $b_{IS}/\sqrt{8}$.[1]

In an established approach to measure distances between a pair of ^{13}C atoms, one of the spins is selectively inverted and the rotor-driven exchange of magnetization is followed in time by collecting a series of 1-D datasets.[3] The trajectory of the difference Zeeman polarization $\langle I_z - S_z\rangle(t)$ may then be simulated to yield the internuclear distance.[1−3] The inherently two-dimensional Zeeman polarization exchange NMR technique has already, at an early stage, been succesfully applied to specifically doubly ^{13}C-labeled retinal in the light-driven ion pump bacteriorhodopsin,[4] which contains a retinoid photochemical energy converter.[5] For the bacteriorhodopsin the rotational resonance technique has been used to discriminate between *s-cis* and *s-trans* conformations, providing for the first time genuine structure information to atomic resolution for an intrinsic membrane protein.[4,6] The bacteriorhodopsin membrane protein is a member of an important class of biological photoreceptors. Another member of the class, rhodopsin,[7] is a G-protein-coupled receptor and responsible for the photochemical energy conversion and the primary steps in visual signal transduction in vertebrates.

The aim of this investigation is to explore the possibility for measuring through-space internuclear distances up to 0.44 nm with high accuracy from the analysis of the rotational resonance line shape, obtained through a single one-dimensional experiment on a di-labeled retinal. The one-dimensional approach to the rotational resonance distance measurements is illustrated and calibrated on a set of doubly labeled compounds, (*all-E*)-[10,20-

[⊗] Abstract published in *Advance ACS Abstracts,* December 1, 1996.
(1) Levitt, M. H.; Raleigh, D. P.; Creuzet, F.; Griffin, R. G. *J. Chem. Phys.* **1990**, *92*, 6347.
(2) Nielsen, N. C.; Creuzet, F.; Levitt, M. H.; Griffin, R. G. *J. Chem. Phys.* **1992**, *96*, 5668.

(3) Raleigh D. P.; Levitt, M. H.; Griffin, R. G. *Chem. Phys. Lett.* **1988**, *146*, 71.
(4) Creuzet, F.; McDermott, A.; Gebhard, R.; van der Hoef, K.; Spijker-Assink, M. B.; Herzfeld, J.; Lugtenburg, J.; Levitt, M. H.; Griffin, R. G. *Science* **1991**, *251*, 783.
(5) Oesterhelt, D.; Stoeckenius, W. *Nature New Biol.* **1971**, *233*, 149.
(6) Thompson, L. K.; McDermott, A. E.; Raap, J.; van der Wielen, C. M.; Lugtenburg, J.; Herzfeld, J.; Griffin, R. G. *Biochemistry* **1992**, *31*, 7931.
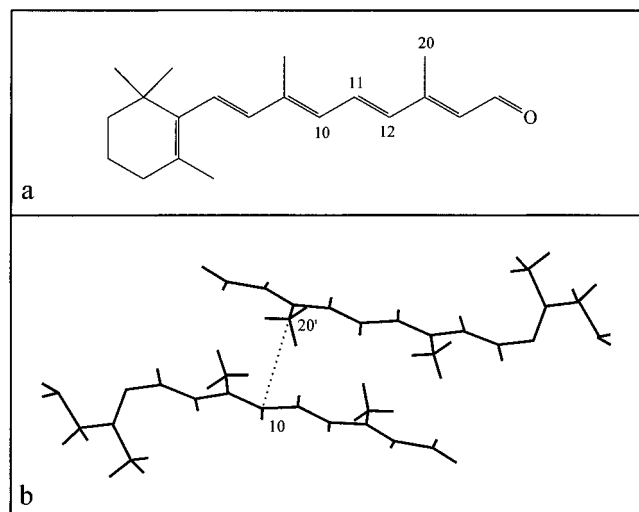(7) Hargrave, P. A.; McDowell, J. H. *FASEB J.* **1992**, *6*, 2323.

Figure 1. (a) Molecular structure of (*all-E*)-retinal, showing the positions labeled for this study. (b) Antiparallel arrangement of (*all-E*)-retinal. The short intermolecular distance $r_{10,20'} = 0.367$ nm is indicated with a dotted line.[8] The ionone ring is not completely resolved.

Table 1. Isotropic Chemical Shifts (σ_i), Anisotropies (δ), Asymmetry Parameters (η), and Pseudotransverse Relaxation Times (T_2') for the Labeled Positions of (*all-E*)-[10,20-$^{13}C_2$]Retinal and (*all-E*)-[11,20-$^{13}C_2$]Retinal

label	σ_i (ppm)	δ (kHz)	η	T_2' (ms)
10	130.1(0.1)	8.1(0.3)	1.0(0.1)	8.3(0.1)
11	134.1(0.1)	−11.3(0.3)	0.7(0.1)	7.5(0.1)
12	133.8(0.1)	8.0(0.3)	1.0(0.1)	7.2(0.1)
20	12.9(0.1)	−1.6(0.3)	1.0(0.1)	10.6(0.1)

Table 2. Observed Splitting ($\Delta\omega_1/2\pi$), Line Width of the Second-Derivative Signal of the $\omega_r/2\pi = 10.0$ kHz Spectrum (Γ), $b_{IS}/2\pi\sqrt{8}$ Calculated from the NMR Data, and Interatomic Distance (r_{IS}) As Deduced from NMR for (*all-E*)-[10,20-$^{13}C_2$]Retinal, (*all-E*)-[11,20-$^{13}C_2$]Retinal, and (*all-E*)-[12,20-$^{13}C_2$]Retinal[a]

compound	$\Delta\omega_1/2\pi$ (Hz)	Γ (Hz)	$b_{IS}/2\pi\sqrt{8}$ (Hz)	r_{IS} (NMR) (nm)	r_{IS}(X-ray) (nm)
10,20 (15%)	12	41	20.8	0.505	0.440
10,20 (100%)	35	45	47.3	0.383	0.367
11,20	78	47	96.7	0.302	0.296
12,20	141	55	169.2	0.250	0.253

[a] For comparison the X-ray distances are also listed.

$^{13}C_2$]-, (*all-E*)-[11,20-$^{13}C_2$]-, and (*all-E*)-[12,20-$^{13}C_2$]retinal. As will be explained below, these compounds provide model distances of 0.253, 0.295, 0.367, and 0.440 nm that are also well-determined by X-ray diffraction structural data of the crystalline (*all-E*)-retinal.[8] In addition, they already provide a coherent set of models for one specific biophysical problem, the characterization of the conformation around the 11-(*Z*) bond of the retinylidene chromophore in the visual signal transduction pigment rhodopsin.[7]

Figure 1a shows the molecular structure of (*all-E*)-retinal, indicating the positions labeled for this study. In Figure 1b, a representation of the relative orientation of two retinal molecules in the crystalline solid state of (*all-E*)-retinal is shown. In this figure the ionone ring is not drawn completely, since structural disorder prevented the determination of all atom positions with X-ray structure determination.[8] Because of the antiparallel spatial ordering, the shortest intermolecular internuclear distance between the 10 and 20′ positions in two different molecules $r_{10,20'} = 0.367$ nm (indicated with a dotted line) is shorter than the intramolecular $r_{10,20} = 0.440$ nm. Hence, for a sample containing dilute highly enriched pairs, the intramolecular coupling will dominate, while the strongest dipolar interaction in a uniform [10,20-$^{13}C_2$]-labeled sample is associated with the intermolecular coupling.

In order to measure distances between the labeled positions in these model compounds, we carefully analyzed resonance line shapes using simulations and fit procedures. To achieve this, high-resolution CP/MAS NMR spectra were recorded for pure [12,20-$^{13}C_2$]-, pure [11,20-$^{13}C_2$]-, pure [10,20-$^{13}C_2$]-, and [10,20-$^{13}C_2$]retinal diluted to 15% in natural abundance retinal at different rotation frequencies of the samples. It is shown that the observed splitting for the $n = 1$ rotational resonance $\Delta\omega_1$ of the vinylic position can be used for all four model compounds to determine r_{IS} using eq 1. Finally, we compare the distances obtained from our MAS NMR investigations with the X-ray structural data.[8]

Materials and Methods

Synthesis of (*all-E*)-[10,20-$^{13}C_2$]retinal, (*all-E*)-[11,20-$^{13}C_2$]retinal, and (*all-E*)-[12,20-$^{13}C_2$]retinal was performed with procedures originally developed by Groesbeek *et al.*,[9] starting from commercially available [1-^{13}C]acetonitrile, [2-^{13}C]acetonitrile, [2-^{13}C]acetic acid, and [^{13}C]-methyl iodide (Cambridge Isotope Laboratories, MA). After silica gel column chromatography purification of the retinal isomer mixture, the (*all-E*)-retinals were crystallized from *n*-pentane at −20 °C. The purity of the labeled retinals was confirmed with 300 MHz ^1H NMR (CDCl$_3$), 75.4 MHz ^1H-noise-decoupled ^{13}C NMR (CDCl$_3$), and mass spectrometry, and the isotope incorporation is >99% at both positions. Subsequently five samples were prepared: pure (*all-E*)-[10,20-$^{13}C_2$]-retinal, pure (*all-E*)-[11,20-$^{13}C_2$]retinal, pure (*all-E*)-[12,20-$^{13}C_2$]retinal, (*all-E*)-[10,20-$^{13}C_2$]retinal diluted to 15% in natural abundance (*all-E*)-retinal, and (*all-E*)-[11,20-$^{13}C_2$]retinal diluted to 15% in natural abundance (*all-E*)-retinal. The dilute samples were prepared from a solution of 15% labeled (*all-E*)-retinal and 85% natural abundance (*all-E*)-retinal (Fluka Switzerland), in *n*-pentane with subsequent recrystallization at −20 °C. All manipulations with isomerically pure retinals were performed in dim red light ($\lambda > 700$ nm) or in the dark. The retinals were stored in an argon atmosphere at −80 °C. Crystalline samples were packed into zirconium oxide rotors with KEL-F caps. CP/MAS NMR experiments were performed with a Bruker MSL 400 spectrometer operating at a ^{13}C frequency of 100.6 MHz, using a 4 mm MAS probe with infrared spinning speed detection. The spinning speed was kept stable within 3 Hz. RAMP cross polarization[10] and continuous wave decoupling with a typical nutation frequency of 80 kHz in the proton channel were used. The spectra of the crystallized retinals were obtained by accumulating approximately 1000 transients with a recycle delay of 1.75 s. The data were collected in 8192 points with a digital resolution of 6 Hz. In one experiment the isotropic chemical shift $\sigma_i = 12.9$ ppm for the C-20 methyl position was referenced to the 1-^{13}C of external singly labeled glycine, which resonates at 176.04 ppm downfield from TMS. Other data are internally referenced to the C-20 shift. The $n = 1$ rotational resonance conditions were determined by fitting the lines of the labeled positions in the $\omega_r/2\pi = 10.0$ kHz spectra with Lorentzians and by taking the difference between the fitted resonance frequencies. Simulations of rotational resonance spectra were performed using the numerical procedures described in ref 1 and 11. Full powder averages were simulated using at least 2000 crystallite orientations. For the comparison in Figure 7, zero filling up to 32k was applied prior to Fourier transformation of the simulated signals. The input parameters are listed in Tables 1 and 2.

Results and Discussion

Figure 2 shows the 100.6 MHz CP/MAS NMR spectra of (*all-E*)-[10,20-$^{13}C_2$]retinal (a, b), (*all-E*)-[11,20-$^{13}C_2$]retinal (c,

(8) Hamanaka, T.; Mitsui, T. *Acta. Crystallogr.* **1972**, *B28*, 214.

(9) Groesbeek, M.; Lugtenburg, J. *Photochem. Photobiol.* **1992**, *56*, 903.
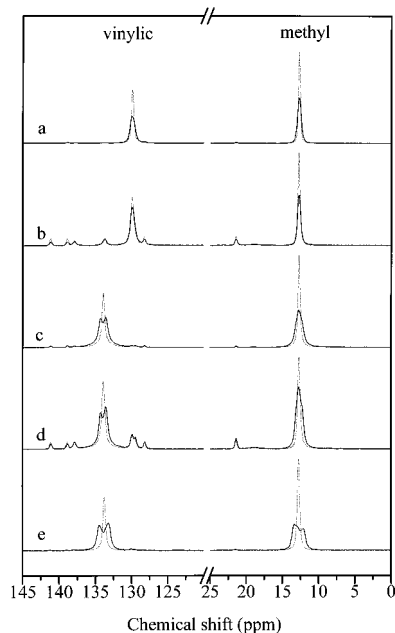
(10) Peersen, O. B.; Wu, X.; Kustanovich, I.; Smith, S. O. *J. Magn. Reson.* **1993**, *104*, 334.

(11) Weintraub, O.; Vega, S.; Hoelger, Ch.; Limbach, H. H. *J. Magn. Reson.* **1994**, *109A*, 14.

Figure 2. Comparison of ^{13}C CP/MAS data at $n = 1$ rotational resonance (solid lines) with data at $\omega_r/2\pi = 10.0$ kHz (dotted lines): well off rotational resonance for pure (*all-E*)-[10,20-^{13}C$_2$]retinal, 99% labeled at both positions (a), (*all-E*)-[10,20-^{13}C$_2$]retinal diluted to 15% in natural abundance (*all-E*)-retinal (b), pure (*all-E*)-[11,20-^{13}C$_2$]retinal 99% dilabeled (c), (*all-E*)-[11,20-^{13}C$_2$]retinal diluted to 15% in natural abundance (*all-E*)-retinal (d), and (*all-E*)-[12,20-^{13}C$_2$]retinal (e).

d), and (*all-E*)-[12,20-^{13}C$_2$]retinal (e). For all five samples spectra were accumulated with $\omega_r/2\pi = 10.0$ kHz (dotted lines) and at the respective $n = 1$ rotational resonance conditions (solid lines). For the [10,20-^{13}C$_2$] samples $\omega_r/2\pi = 11.794(2)$ kHz, for the [11,20-^{13}C$_2$] samples $\omega_r/2\pi = 12.198(2)$ kHz, and for the [12,20-^{13}C$_2$] sample $\omega_r/2\pi = 12.180(2)$ kHz at the $n = 1$ rotational resonance condition. The data in Figure 2 are scaled in order to keep the integrated intensities of the signals approximately equal at the different spinning speeds. The effect of the rotor-driven dipolar recoupling on the $n = 1$ line shape is now evident. The resonances of the $n = 1$ spectra are broadened compared to the 10.0 kHz spectra, and additional fine structure is observed for the [11,20-^{13}C$_2$] and [12,20-^{13}C$_2$] compounds. The $n = 1$ spectra of the [10,20-^{13}C$_2$] sample show a broadening of the signals, but no additional fine structure. The dipolar recoupling effects are more pronounced for (*all-E*)-[11,20-^{13}C$_2$]- and -[12,20-^{13}C$_2$]retinal since the $r_{11,20} = 0.296$ nm and the $r_{12,20} = 0.253$ nm are considerably smaller than $r_{10,20} = 0.440$ nm.

If the spin pair involves a methyl and a vinylic carbon, $\Delta\omega_{IS} \gtrsim |\delta_I| + |\delta_S|$, the sum of the absolute values of the chemical shift anisotropies. To first order a splitting of the resonance at the $n = 1$ rotational resonance condition is expected for the stronger dipolar couplings. Since the dipolar interaction is symmetric in the two spins, a similar rotational resonance line shape for both label signals, for $n = 1$, is in principle expected in the case of small shift anisotropy.[1]

In Figure 2c, d the C-11 resonance is apparently a doublet, but the C-20 line shape is more complicated. It is immediately obvious that for the [11,20-^{13}C$_2$] compound only the response from the vinylic C-11 resonance is in line with the generally accepted theory, which predicts a neat splitting of both lines.[1] For the [12,20-^{13}C$_2$] compound both labeled sides of the $n = 1$ rotational resonance give rise to a doublet type contribution to the spectrum, although the C-20 response appears distorted.

The $n = 1$ experimental data can be compared with theoretical predictions in detail to address the applicability of the theoretical
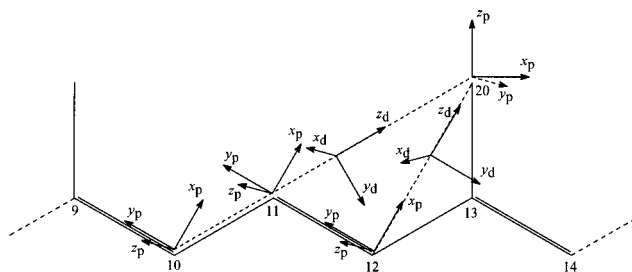

Figure 3. Approximate orientation of the reduced CSA tensors for the C-10, C-11, C-12, and C-20 positions and the dipolar coupling tensors in the labeled (*all-E*)-retinals.

approaches and to calibrate a method for measuring distances. It should be stressed here that the parameters used for these simulations are not fitted to the rotational resonance data, but are from independent sources. All parameters used for the simulations are from X-ray and separate MAS experiments and are listed in Tables 1 and 2. The isotropic chemical shifts σ_i were measured by fitting the MAS centerbands for the $\omega_r/2\pi = 10.0$ kHz datasets with Lorentzians. The anisotropy parameters δ and η were obtained by a Herzfeld–Berger analysis[12] of datasets collected with $\omega_r/2\pi = 2.149$ kHz, $\omega_r/2\pi = 1.564$ kHz, and $\omega_r/2\pi = 1.937$ kHz for the [10,20-^{13}C$_2$], [11,20-^{13}C$_2$], and [12,20-^{13}C$_2$] compounds, respectively (data not shown). Pseudotransverse relaxation times T_2' used for the simulations were estimated from the Lorentzian line widths Γ at $\omega_r/2\pi = 10.0$ kHz according to $T_2' = (\pi\Gamma)^{-1}$. For all the compounds used in our study, the J couplings are very small and can be neglected. In the rotational resonance simulations, the dipolar coupling b_{IS} is calculated from the internuclear distance using eq 1. A right-handed principal axis frame for the dipolar coupling tensor was taken as the frame of reference with the positive z axis along the vector connecting the vinylic and C-20 atoms and the y axis perpendicular to the x axis in the conjugated plane (Figure 3). The orientations of the principal axis frames of the chemical shift tensors with respect to the molecular frame are not known exactly. For a vinylic carbon, the σ_{11} axis, corresponding to the most upfield principal component, is almost perpendicular to the plane of conjugation. The σ_{33} axis, for the most downfield component, is approximately in the conjugated plane perpendicular to the double bond, and finally the σ_{22} axis is along this bond (see, e.g., Veeman[13]). To obtain the reduced tensor elements for the simulations, σ_{xx}, σ_{yy}, and σ_{zz}, with $|\sigma_{zz}| \geq |\sigma_{xx}| \geq |\sigma_{yy}|$, the isotropic chemical shift σ_i was subtracted and the principal axis components were rearranged.

The resulting orientations of the principal axes for C-12, C-11, and C-10 are also depicted in Figure 3. The effect of the methyl anisotropy on the line shape is negligable since $\Delta\omega_{IS}$ is much larger than the methyl anisotropy δ_S. An approximate orientation of the principal axis frame for the 20-methyl was inferred from the various compilations of chemical shift anisotropy data presented in the literature,[13,14] indicating that the σ_{11} axis should be roughly along the chemical bond, while the σ_{33} axis is most likely perpendicular to the bond in the plane of the molecule. This choice parallels earlier rotational resonance investigations.[4] After subtraction of σ_i and rearrangement of the principal components, the principal axis frame orientation depicted in Figure 3 results.

(12) de Groot, H. J. M.; Smith, S. O.; Kolbert, A. C.; Courtin, J. M. L.; Winkel, C.; Lugtenburg, J.; Herzfeld, J.; Griffin, R. G. *J. Magn. Res.* **1991**, *91*, 30. Herzfeld, J.; Berger, A. E. *J. Chem. Phys.* **1980**, *73*, 6021.
(13) Veeman, W. S. *Prog. NMR Spectrosc.* **1984**, *16*, 193.
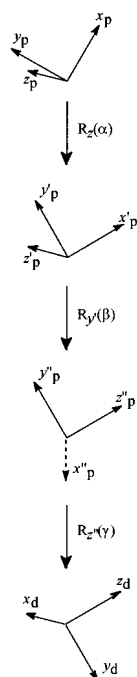(14) Mehring, M. *Principles of High Resolution NMR in Solids*, 2nd ed.; Berlin, 1983.

Figure 4. Stepwise derivation of the Euler angles (α, β, γ) for the vinylic carbons illustrating the transformation of the principal axis frame (x_p, y_p, z_p) into the dipolar reference frame (x_d, y_d, z_d).

Figure 4 illustrates the stepwise derivation of the Euler angles for the vinylic carbons that are required to transform the chemical shift tensor frames into the dipolar reference frame. Following standard conventions,[15] where for a set of Euler angles (α, β, γ) the $R(\alpha, \beta, \gamma) = R_{z''}(\gamma) R_{y'}(\beta) R_z(\alpha)$, it is easily seen from Figure 4 that $R(-30, 90, 180)$ transforms the principal axis frame of the 10 and 11 vinylic carbons into the appropriate dipolar frame. Using a similar procedure, it can be deduced that $R(0, -60, -90)$ represents the rotation needed to transform the methyl principal axis frame into the dipolar reference frame. For the $[12,20\text{-}^{13}C_2]$ labels it is $R(0, 90, 180)$ and $R(0, -30, -90)$ that transform the shift frames of C-12 and C-20 into the dipolar frame. Finally, for the pure $[10,20\text{-}^{13}C_2]$retinal, in which the intermolecular coupling dominates, the orientation of the dipolar tensor and therefore the reference frame is different from that in the case of dilute $[10,20\text{-}^{13}C_2]$retinal. The deviation of the vector connecting C-10 and C-20' and the z_p axis for C-10 is within the error of determining the Euler angles associated with the uncertainties in the shift tensor orientations, and the dipolar reference frame was chosen to coincide with the principal axis frame of the C-10 vinylic carbon. In that case, the orientation of the principal axis frame for C-10 is the same as for the dipolar reference frame, while $R(-90, 90, -30)$ transforms the principal axis frame of C-20' into the reference frame.

For the vinylic carbons, deviations up to ~15° from the reference frames indicated in Figure 3 may occur, while for the 20-methyl, the deviation may still be larger. However, since $\Delta\omega_{IS} \gtrsim |\delta_I| + |\delta_S|$, the effect of the anisotropy on the rotational resonance line shapes is only minor. This was verified by calculating theoretical predictions for the line shapes using different values for the parameters. In particular, simulations with different sets of Euler angles were generated, giving almost negligable differences in the spectra.

For instance, a comparison between experimental data for the C-11 position and simulations is illustrated in Figure 5. In
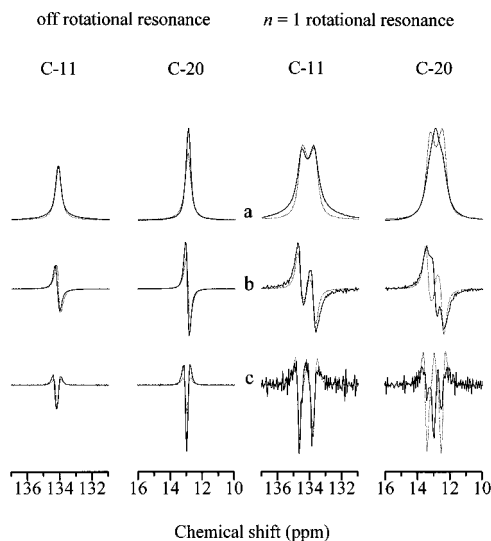

Figure 5. ^{13}C CP/MAS NMR data (solid lines) and simulations (dotted lines) for pure (*all-E*)-$[11,20\text{-}^{13}C_2]$retinal at $\omega_r/2\pi = 10.0$ kHz and $\omega_r/2\pi = 12.198$ kHz, the $n = 1$ rotational resonance: (a) spectrum, (b) first derivative, and (c) second derivative.

this figure, the signals of the vinylic and methyl labels are shown, with $\omega_r/2\pi = 10$ kHz and at $n = 1$ rotational resonance. In addition, the first and second derivatives of the signals are plotted. All resonances are scaled so that the amplitudes of the C-11 resonances coincide. For the vinylic C-11 the agreement between the data and simulations is quantitative with respect to the positions of the maxima and qualitative with respect to the overall line shape.

From the comparison of the experimental results with the simulated data in Figure 5, it is evident that it is impossible to simulate the experimentally observed line shapes of both spins in detail for internuclear distances in the 0.3 nm range with the rotational resonance theory that was originally developed for the description of this phenomenon within a dilute spin pair, for short internuclear distances and correspondingly strong dipolar couplings, as for adjacent carbons in one molecule.[1] A similar conclusion was reached independently by Peersen *et al.*[16] who studied the rotational resonance effects for pairs of nuclei in a small peptide.

The $n = 1$ second-derivative line shape for the methyl side apparently contains an off rotational resonance type single line, superimposed on the $n = 1$ rotational resonance "doublet". The discrepancies between experiment and isolated spin-pair theory for the methyl response originate from additional field-dependent interactions interfering with the very weak homonuclear dipolar couplings. For instance, the linewidths for the two labels are different, and for the $\omega_r/2\pi = 10$ kHz data the vinylic resonance has extended wings at its bottom, which are not reproduced by the theory. In contrast, the methyl side of the spin pair response is much narrower. Interestingly, the separation between the two outer lines in the second-derivative methyl response at rotational resonance matches the simulations and the characteristic splitting of the vinyl part (Figure 5c). In this investigation we focus on the extrema and $\Delta\omega_1$. A discussion of the details of the line shape is beyond the scope of the present study, and will be reported elsewhere.

Interestingly, despite the obvious differences between the experimental data and the theoretical predictions with respect to the overall line shape, the $\Delta\omega_1$ matches the simulations quite well. To enhance the extrema for further analysis, we now often

(15) Spiess, H. W. In *NMR Basic Principles and Progress;* Diehl, P., Fluck, E., Kosfeld, R., Eds.; Springer-Verlag: Berlin, 1978; Part 15.

(16) Peersen, O.; Groesbeek, M.; Aimoto, S.; Smith, S. O. *J. Am. Chem. Soc.* **1995**, *117*, 7228.
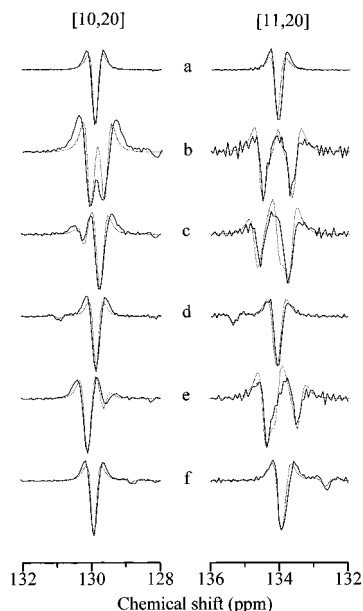
Figure 6. Comparison of second derivatives of experimental data (solid lines) and simulations (dotted lines) for pure (*all-E*)-[10,20-$^{13}C_2$]retinal and pure (*all-E*)-[11,20-$^{13}C_2$]retinal with $\omega_r/2\pi = 10.0$ kHz (a), at $n = 1$ rotational resonance (rr), +25 Hz off rr (c), +100 Hz off rr (d), −25 Hz off rr (e), and −100 Hz off rr (f).
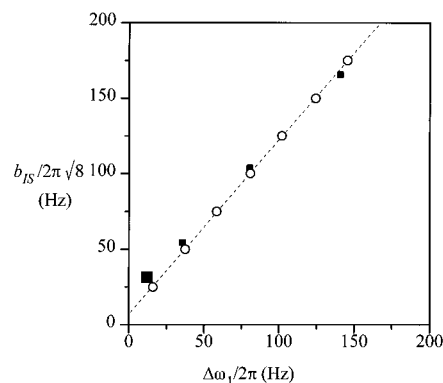

Figure 7. $b_{IS}/2\pi\sqrt{8}$ from X-ray determination versus $\Delta\omega_1/2\pi$ of the vinylic resonances measured from the NMR spectra of the four model compounds (■). The size of the squares represents the estimate of the statistical errors for both experimental procedures. The solid line represents a linear fit to the simulated points (○) and corresponds to $b_{IS}/2\pi\sqrt{8} = 1.15(\Delta\omega_1/2\pi) + 7$ (Hz).

use second derivatives of the data and the corresponding simulations. This is illustrated in Figure 6, which shows the second derivatives of the experimental data (solid lines) and simulations (dotted lines) for pure (*all-E*)-[10,20-$^{13}C_2$]retinal and pure (*all-E*)-[11,20-$^{13}C_2$]retinal at six different rotation frequencies ($\omega_r/2\pi = 10.0$ kHz, the $n = 1$ rotational resonance condition, 25 and 100 Hz above the $n = 1$ rotational resonance condition and 25 and 100 Hz below the $n = 1$ rotational resonance condition). It is clear that the minima in all six second derivative datasets are satisfactorily reproduced by the simulations. In Figure 6b, for the $n = 1$ rotational resonance condition, the splittings in the second derivative of the data are in fact remarkably well reproduced by the simulations.

At $n = 1$ rotational resonance, for pure (*all-E*)-[10,20-$^{13}C_2$]-retinal the change in line shape of the C-10 signal is now also due to a combination of intramolecular and intermolecular couplings, since $r_{10,20'} < r_{10,20}$. The minima in the experimental data are accurately represented by the minima of the theoretical line calculated for the intermolecular distance, in agreement with expectations.

It is thus concluded that the apparent splitting in the vinylic resonances is due to dipolar recoupling at the rotational resonance condition. This information may be used to determine distances between two spins. For model compounds like (*all-E*)-retinal the analysis of experimental data with the help of simulations is definitely the most elegant and probably the most accurate way of measuring the internuclear distance directly from the second-derivative data. However, when the method is applied to systems where the spin pairs are very dilute, like, for instance, in membrane proteins, the relevant information needs to be extracted from a noisy background containing contributions from natural abundance signals that may be several times stronger than the signals from the labels. The next step in our analysis procedure is therefore to investigate if it is possible to extract the splitting $\Delta\omega_1$ from the second-derivative data using straightforward iterative fitting with the second derivative of a pair of Lorentzian lines and to verify if the splittings measured in this way still reproduce the $\Delta\omega_1$ predicted by the full computer simulations. First, σ_i and Γ for the $\omega_r/2\pi$

= 10.0 kHz resonance were determined by fitting the second derivatives of the signals using Lorentzian lines. Then, for pure [12,20-$^{13}C_2$]-, [11,20-$^{13}C_2$]-, and [10,20-$^{13}C_2$]retinal, fitting the two maxima in the second derivative of the $n = 1$ line shapes while keeping Γ constant yields $\Delta\omega_1$ with an accuracy of at least the digital resolution. This procedure ensures an optimal accuracy for the measurement of $\Delta\omega_1$ for these model compounds (Table 2). The experimental error associated with the data points is estimated as $\sim$4 Hz. Obviously, the accuracy is improved by the interpolation from the fitting procedure, relative to simply determining the positions of the minima by reading off the extrema with the absolute accuracy of the digital resolution in the spectra.

For dilute [10,20-$^{13}C_2$]retinal the effect of the dipolar recoupling due to the relatively large internuclear distance $r_{10,20'}$ = 0.440 nm is so small that accurate analysis in the previously described way is not possible. Moreover, the relatively large natural abundance background signal comprises an important part of the total response. In this case $\Delta\omega_1$ could be determined by analyzing the resonance line shape instead of its second derivative. First, a spectrum collected with a spinning speed 100 Hz less than the $n = 1$ rotational resonance condition was carefully fitted with a superposition of Lorentzian lines. For dilute [10,20-$^{13}C_2$]retinal at least four Lorentzians are required, one strong component for the contribution from the label and three weaker components to generate the natural abundance background in the spectral region of 10-^{13}C. Subsequently, a dataset with the spinning speed exactly at rotational resonance is analyzed while allowing for additional broadening of the Lorentzian representing the label response slightly off rotational resonance. The parameters describing the other Lorentzians in the fit are kept identical to the values determined for the data off rotational resonance. Hence, the only free parameter in this second fitting procedure is the line width of the contribution from the label. Both fitting procedures are illustrated in the Supporting Information. The increase of the line width, with respect to the response off rotational resonance, provides a fair estimate of the $\Delta\omega_1$ due to the rotational resonance dipolar recoupling.

Finally, in Figure 7 a graph of the $b_{IS}/\sqrt{8}$ in the compounds versus the $\Delta\omega_1$ is presented. To compare these data with the rotational resonance theory, a series of $n = 1$ rotational resonance second-derivative simulations was performed, with 10 Hz < $b_{IS}/2\pi\sqrt{8}$ < 190 Hz (see the Supporting Information). It appears that $\Delta\omega_1$ in the simulations varies linearly with $b_{IS}/\sqrt{8}$, according to the solid line in Figure 7, and can be described
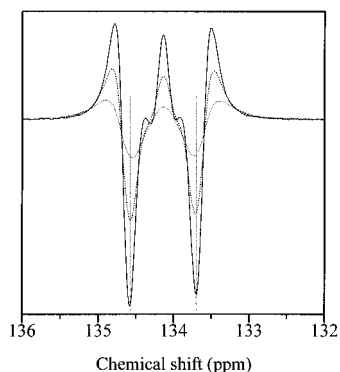
Figure 8. Simulated vinylic line shapes for different 5 ms $< T_2' <$ 10 ms, using the parameter set from the analysis of the [11,20-$^{13}C_2$]retinal spectra: solid line, $T_2' = 10$ ms; dashed line, $T_2' = 7$ ms; dotted line, $T_2' = 5$ ms. The dotted straight lines indicate the positions of the extrema of the $T_2' = 10$ ms line.

by $b_{IS}/2\pi\sqrt{8} = 1.15 \ (\Delta\omega_1/2\pi) + 7$ (Hz) to a very good approximation.

It can be emphasized that the offset and slope are the result of and implicit in the exact numerical simulations for the two-spin system. In particular, they should not be interpreted as an empirical correction to the data or eqs 1−3. In Figure 7 the squares represent the experimental data. The simulations depicted by open circles are strictly independent from these measurements. Therefore, both measured and simulated values of $\Delta\omega_1$ thus appear to be systematically smaller than predicted by the first-order theory in eqs 1−3. This is attributed mainly to the T_2-type line broadening of the rotational resonance response that decreases the separation between the singularities of the first-order theory and gives rise to rounded, inward shifted maxima (Figure 8). As already mentioned before, this effect is taken into account in the spin-pair simulations through apodization with a pseudo T_2' exponential broadening factor in the time domain before the Fourier transform (Figure 6).

The simulated points in Figure 7 are not very sensitive to small variations of the linewidth and, correspondingly, the pseudo T_2'. This is illustrated in Figure 8, which shows a set of simulations, using the parameters from the [11,20-$^{13}C_2$] analysis and 5.0 ms $< T_2' <$ 10.0 ms. Although the line shapes change considerably, the locations of the maxima stay the same within the digital resolution of these simulations. The line in Figure 7 represents a fit to the simulated points and may serve as a good calibration for measuring distances from $n = 1$ rotational resonance spectra in our labeled retinals, since for practical purposes a simple expression, $b_{IS}/2\pi\sqrt{8} = 1.15(\Delta\omega_1/2\pi) + 7$ (Hz), can now be used instead of full numerical simulations. Applying this calibration, distances can be calculated for the set of model compounds which are listed in Table 2. For pure [10,20-$^{13}C_2$]-, [11,20-$^{13}C_2$]-, and [12,20-$^{13}C_2$]retinal, the results are in close agreement with the X-ray data, as can already be expected on the basis of the close correspondence between the data and simulations in Figure 6 with respect to the splittings. The estimated accuracy of ±4 Hz for the

determination of $\Delta\omega_1/2\pi$ contributes ±0.005 nm to the error in the distance. Additional systematic errors arising from the deviation between the line in Figure 7 and the experimental points yield an overall error estimate of ∼±0.01−0.02 nm for distances below 0.4 nm.

It thus appears that a determination of the location of the maxima associated with the singularities in the rotational resonance line shape provides a good route to the measurement of homonuclear dipolar interactions in the quasi-two-spin system at rotational resonance and internuclear distances. In this respect, peaks and shoulders in a spectrum are generally considered a source of valuable information, even when the associated spectral lines are heavily distorted, also, e.g., in optical spectroscopy.

In our study we have chosen to evaluate the particular problem of measuring distances between vinylic carbons and methyl carbons in some depth, from a practical perspective and aiming for an optimization with respect to accuracy. Other investigations that have been performed in the past have largely neglected the possibility for extracting distances from the analysis of rotational resonance line shapes, in favor of magnetization exchange experiments. The results presented here suggest that line shape analysis will be quite useful for pairs of carbons provided that essential features of the response can be described in terms of the two-spin approximation. Testing with model compounds may help to determine the accuracy that may be achieved for other specific cases, involving different types of carbons.

Conclusion

The results discussed in this paper show that it is possible to measure the internuclear distance between a vinylic and a methyl carbon in doubly labeled retinals accurately from the apparent splitting in a 1-D rotational resonance dataset. A calibration procedure is worked out and tested for four independent model distances. The advantage of this technique over the more widely used magnetization exchange experiments is that the distance information can be obtained in a single experiment and can already be extracted using straightforward fitting procedures. It should be possible to use this approach for collecting structural constraints in complex systems, for instance ligands bound to receptor proteins.

Supporting Information Available: Figures showing measurements of the apparent splitting in the experimental data, the effect of dipolar coupling, and simulations of a series of $n = 1$ rotational resonance spectra (3 pages). See any current masthead page for ordering and Internet access instructions.

JA961475M